Research Article

Slip Effect Study of 4:1 Contraction Flow with Rounded Corner Geometry for Newtonian Fluid

Nawalax Thongjub* and Vimolrat Ngamaramvaranggul
Department of Mathematics and Computer Science, Faculty of Science,
Chulalongkorn University, Bangkok 10330, Thailand

Bumroong Puangkird
Department of Mechanical Engineering, Faculty of Engineering,
King Mongkut's Institute of Technology Ladkrabang, Bangkok 10520, Thailand

Abstract

The simulation of slip effect for 4:1 contraction problem with rounded corner geometry for Newtonian fluid is determined to study kinematic behaviors from streamline path, shear stress values and vortex size by a model of Navier-Stokes equation. Two-dimensional planar isothermal incompressible creeping flow with slip and no slip condition is considered with a semi-implicit Taylor-Galerkin pressure-correction based on the finite element method. The streamline-Upwind/Petrov-Galerkin and velocity gradient recovery schemes are employed to stabilize the converged solution. The slip velocity is computed after each time step and the modification of slip coefficient is adjusted to proper slip velocity in order to reduce the vortex size and stress along the channel wall. Finally, the best mesh is selected to run for the final solution and the slip condition of Phan-Thien slip rule on the channel wall is done to get the result to be in better agreement with experiment.

Keywords: Slip effect; 4:1 contraction flow; Phan-Thien slip rule; Slip coefficient.

1. Introduction

The research focuses on the slip effect of 4:1 contraction flows for Newtonian fluids upon a semi-implicit Taylor-Galerkin pressure-correction finite element method (STGFEM) for two-dimensional planar system. To investigate kinematic behaviors of strong elongation and violent shear stress abrupt contraction, a fluid passes a sudden change in geometry. The slip effect is used to study in rounded corner 4:1 contraction domains in order to reduce the shear stress at sharp corners.

For the experimental work, Walters and Rawlinson [1] implemented the apparatus of planar contraction flows for Boger fluid. In1987, Boger [2] compared the numerical solution and the experimental result of circular contraction for both Newtonian and Non-Newtonian fluids.

To avoid complex analytic solution of viscoelastic problems, the simulation of the mathematical model for the non-linear partial differential equations that are derived from conservation of mass and momentum is set up to solve problems. The numerical techniques are employed to calculate an approximate solution. There are a variety of numerical methods such as finite element method (FEM), finite volume method (FVM) and finite difference method (FDM). In 1999, Phillips and Williams [3] solved a 4:1 planar

***Correspondence** : t_nawalax@hotmail.com

contraction of Oldroyd-B fluids for creeping and inertial flows by a semi-Lagrangian FVM. After that, they [4] expanded the coordinate system to axisymmetric flows. Eulerian methods were used to fix the grids. Aboubacar et al. [5, 6] stated that a cell-vertex hybrid finite volume/element method is appropriate for computing Oldroyd-B and Phan-Thien/Tanner (PTT) fluids with both rounded and sharp corner contraction flows. Alves et al. [7] computed the creeping PTT flow past planar abrupt contractions via FVM and showed that Deborah numbers and contraction ratios influence the flow behavior. In 2001, Ngamaramvaranggul and Webster [8] applied the FEM to solve the Oldroyd-B problem for stick-slip flows and they adjusted the boundary after die exit using the free surface method for die-swell flows. They showed that the swelling ratio depended on a function of relaxation time. Consequently, they [9] solved a problem of pressure-tooling wire-coating flows with Phan-Thien/Tanner fluid using standard FEM including the streamline-upwind Petrov/Galerkin (SUPG) method that stabilized the converged solution.

Experimental and numerical data in studies of fluid flows through solid walls have shown that the slip velocity appears on solid surfaces. In addition, a number of studies have applied various numerical methods to estimate the slip velocity at the walls. Silliman and Scriven [10] illustrated the slip effect for free surfaces. Ramamurthy [11] concentrated on the surface melt fracture of HDPE and LLDPE results from slip in die. Phan-Thien [12] studied the slip at solid walls by setting the slip velocity as a function of wall shear stress while the critical shear stress is less than wall shear stress. In 2000, Ngamaramvaranggul and Webster [13] compared the solution of various slip effect schemes for free surfaces in tube-tooling and pressure-tooling die problems.

In this study, the slip condition is employed in the problem of 4:1 contraction for Newtonian fluids under the two-dimensional planar isothermal incompressible flows. A semi-implicit Taylor-Galerkin pressure-correction finite element method separates the Navier-Stokes equation into a system of simple linear equations, and all solutions have been stabilized by means of the streamline-upwind Petrov/Galerkin and velocity gradient recovery techniques. The solutions for slip and no-slip conditions are compared after the optimum value of the slip coefficient with rounded corner geometries is found.

2. Governing Equations

The conservations of mass and momentum for incompressible viscoelastic flow under non-gravity conditions are preserved in the Navier-Stokes equations with unit component while many other studies have been presented in non-dimensional systems. Thus, the normalization of unit is proposed. As a result of standard comparison, the derivative equations of continuity equation (1) and kinematic equation (2) is transformed into a dimensionless system as

$$\nabla \cdot \boldsymbol{U} = 0 \tag{1}$$

$$\mathrm{Re}\frac{\partial \boldsymbol{U}}{\partial t} = \nabla \cdot \boldsymbol{T} - \mathrm{Re}\boldsymbol{U} \cdot \nabla \boldsymbol{U} - \nabla \vec{P} \tag{2}$$

where $\boldsymbol{U}$ is velocity vector, $\boldsymbol{T}$ is the extra-stress tensor $\boldsymbol{T} = \boldsymbol{\tau} + 2\mu_2 \boldsymbol{D}$, $\boldsymbol{\tau}$ is the polymeric component of $\boldsymbol{T}$, the deformation tensor rate is $\boldsymbol{D} = \frac{(\nabla \boldsymbol{U} + \nabla \boldsymbol{U}^t)}{2}$, and $\vec{P}$ is pressure.

The Reynolds number is denoted by $\mathrm{Re} = \frac{\rho V L}{\mu_0}$. Here, ρ is the density, V is the characteristic velocity, and L is the

characteristic length. μ_0 is the zero-shear viscosity, and $\mu_0 = \mu_1 + \mu_2$ where μ_1 is the polymeric viscosity and μ_2 is the solvent viscosity. In order to compare our results with those of [5,6] at the same condition, we definded the non-dimensional parameters as $\mathrm{Re} = 0$, $\frac{\mu_1}{\mu_0} = 0.88$, and $\frac{\mu_2}{\mu_0} = 0.12$.

3. Numerical Scheme

Non-linear differential equations are often solved using the numerical methods employed in this peper, namely the basic FEM. The convected equation (2) is computed by STGFEM that has three time stages each of which is discretized into a system of linear equations.

3.1 Semi-implicit Taylor-Galerkin pressure- correction finite element method

The factional time steps and FEM are employed to split the non-dimensional Navier Stokes equation (2) into three stages per time step. This convenient technique is known as the semi-implicit Taylor-Galerkin pressure-correction finite element method and is shown below.

Step 1a :

$$\frac{2\mathrm{Re}}{\Delta t}(\boldsymbol{U}^{n+\frac{1}{2}} - \boldsymbol{U}^n) = \nabla \cdot \mu_2 (\boldsymbol{D}^{n+\frac{1}{2}} - \boldsymbol{D}^n) \quad (3)$$
$$+ \left[\nabla \cdot \left(\boldsymbol{\tau} + 2\mu_2 \boldsymbol{D} \right) - \mathrm{Re}\boldsymbol{U} \cdot \nabla \boldsymbol{U} - \vec{P} \right]^n$$

Step 1b :

$$\frac{\mathrm{Re}}{\Delta t}(\boldsymbol{U}^* - \boldsymbol{U}^n) = \left[\nabla \cdot \boldsymbol{\tau} - \mathrm{Re}\boldsymbol{U} \cdot \nabla \boldsymbol{U} \right]^{n+\frac{1}{2}} \quad (4)$$
$$+ \left[\nabla \cdot (2\mu_2 \boldsymbol{D}) - \nabla \vec{P} \right]^n + \nabla \cdot \mu_2 (\boldsymbol{D}^* - \boldsymbol{D}^n)$$

Step 2 :

$$\nabla^2 (\vec{P}^{n+1} - \vec{P}^n) = \frac{2\mathrm{Re}}{\Delta t} \nabla \boldsymbol{U}^* \quad (5)$$

Step 3 :

$$\frac{2\mathrm{Re}}{\Delta t} (\boldsymbol{U}^{n+1} - \boldsymbol{U}^*) = - (\vec{P}^{n+1} - \vec{P}^n) \quad (6)$$

The partial differential equations (1)-(2) are separated by FDM and FEM. The derivative term of time is determined with the Taylor series, and the spatial terms are considered with the weight residual of the Galerkin finite element method. Then the equations of stages (3)-(6) are converted into a system of linear equations. Finally, the steps 1 and 3 are solved with Jacobi iterative method whilst step 2 is approximated using the Cholesky decomposition algorithm.

3.2 Phan-Thien slip rule

To fit the slip velocity, Phan-Thien [12] demonstrated the concept of slip velocity as a function of wall shear stress that is close to an experimental solution. This scheme is helpful to reduce shear stress for an abrupt contraction, and consequently the slip velocity is calculated when the wall shear stress becomes greater than a critical shear stress.

$$V_{slip} = V_{mean} \left[1 - \exp(- \alpha \frac{\tau_w}{\tau_{crit}}) \right] \quad (7)$$

where V_{slip} is the slip velocity, V_{mean} is the mean velocity of the flowrate for a no-slip case, α is the slip coefficient, τ_w is the wall shear stress, and τ_{crit} is the critical shear stress.

4. Problem Specification

In industrial processes, especially for 4:1 contraction problems, there are many obstacles when fluid passes through a part of an abrupt contraction. Thus, the geometrical domain of this problem for sharp corners [14] is changed to rounded corners as shown in Figure 1. The downstream half channel width of planar 4:1 contraction at entry and exit sections are $27.5L$ and $49L$, respectively. At the inlet entry, fluid flow is set to be the Poiseuille flow in a channel length that is long enough for developing a

parabolic flow at the exit section. At the channel wall, the slip condition is added to compute the slip velocity that appear in real problems.

$$u(y)=\frac{3}{128}(16-y^2) \quad (8)$$

$$v = 0 \quad (9)$$

$$\tau_{xx} = 2We\mu_1\left(\frac{\partial u}{\partial y}\right)^2 \quad (10)$$

$$\tau_{yy} = 0 \quad (11)$$

$$\tau_{xy} = \mu_1 \frac{\partial u}{\partial y} \quad (12)$$

where velocity u in x-direction depends on the y-component, and velocity v in the y-direction vanishes. The normal stress τ_{xx} depends on the shear rate τ_{xy} while the normal stress τ_{yy} is zero.

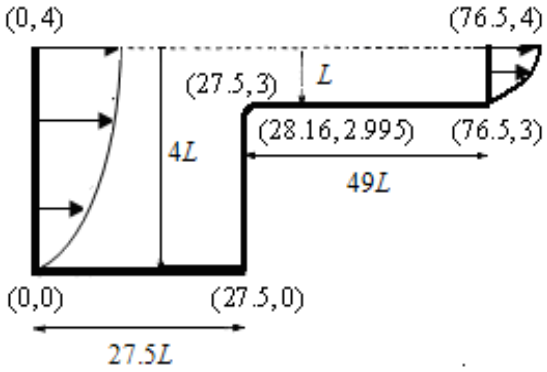

Fig.1. Schematic of 4:1 contraction flow for rounded corners.

The rounded geometry is generated by Aboubacar et al. [6,7] with a curve segment at contraction to reduce the severe stress. There are three different meshes labelled as mesh1, mesh2 and mesh3 for coarse, medium, and fine meshes, respectively, as shown in Figure 2. The mesh pattern of all types as declared in Table 1 is generated as a bias triangular element. The tiny elements ($h_{\min}$) are set up near rounded corners.

Table 1. Mesh characteristics of rounded corners.

Meshes	Elements	Nodes	Degree of freedom	$h_{\min}$
mesh1	1626	3433	18069	0.017
mesh2	2693	5652	29740	0.010
mesh3	4751	9790	51470	0.006

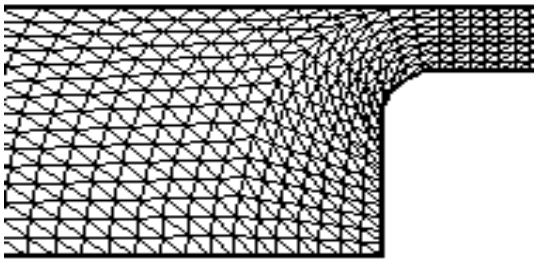

(a) mesh1

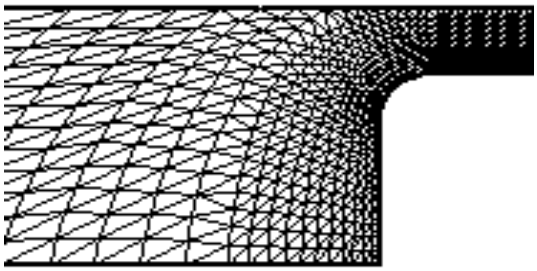

(b) mesh2

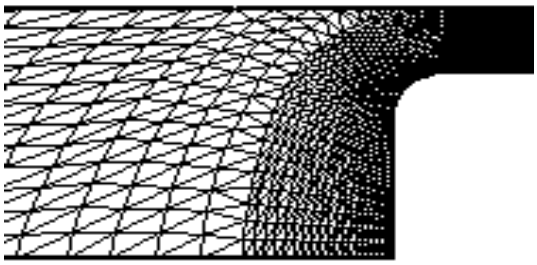

(c) mesh3

Fig.2. Rounded mesh pattern of 4:1 contraction flow.

5. Results

To find the proper mesh for

displaying final solution, we compared solutions for all mesh types in order to reduce computing time. After the best mesh was chosen, it was applied to operate in the Newtonian problem under the no-slip and slip conditions.

Table 2. The peak values of Newtonian fluids on the bottom downstream wall with noslip for rounded corner meshes.

Meshes	τ_{xx}	τ_{xy}	τ_{yy}	$\dot{\gamma}$
mesh1	7.177	3.542	0.261	3.734
mesh2	7.447	3.698	0.265	3.888
mesh3	7.955	3.905	0.252	4.034

A stick or no-slip problem is studied by collecting the stresses and the shear rate. The highest values of the normal stress, the shear stress and the shear rate $\dot{\gamma}$ on the bottom downstream wall are shown in Table 2. We found that the peak values of all of the meshes were similar and depended on the element sizes. The tendency of the highest values for the stresses and the shear rate versus the mesh acuteness in Table 2 are similar except for the value of τ_{yy} for mesh3 which is less than that of mesh1 and that of mesh2. The results of mesh2 and mesh3 are close. The program used the computing time to access mesh2 less than that of mesh3 as comparison in previous work [15]. Thus, mesh2 is chosen as a model for the final solution.The trend of the second invariant (II) and the shear rate ($\dot{\gamma}$) are similar as depicted in Figure 3. Now, the slip condition is initiated to compute the slip velocity from critical II to find the optimal slip coefficient (α) by assuming the values of the slip coefficient. Under a complete slip, we first set α to 1 in order to choose the critical II then various choices of II between 2.3 and 3.6 is determined as depicted in Figure 4. We found that the critical value of II was 2.3, which made the peak of the shear rate grow to 3.857, which is the lowest value when compared with the other peak values of II as shown in Figure 5. Using the critical II to decide the optimum α, the minimum shear rate is displayed by α=0.1 as illustrated in Figure 6. Additionally, the shear rates of α at 0.1, 0.2, 0.4 and 1.0 widely oscillated. We found that the values for the shear rate are high when the second invariant value increases along with the slip coefficient value.

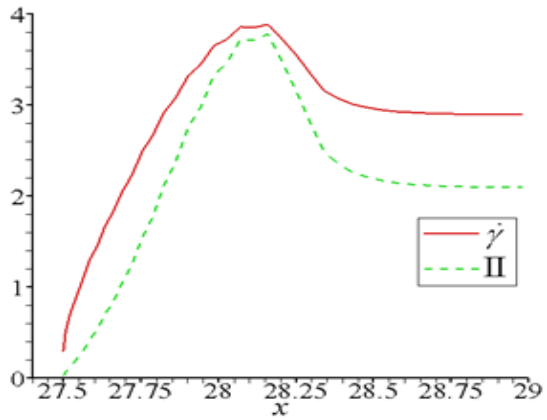

Fig.3. II and $\dot{\gamma}$ along downstream wall with no slip, Newtonian fluid.

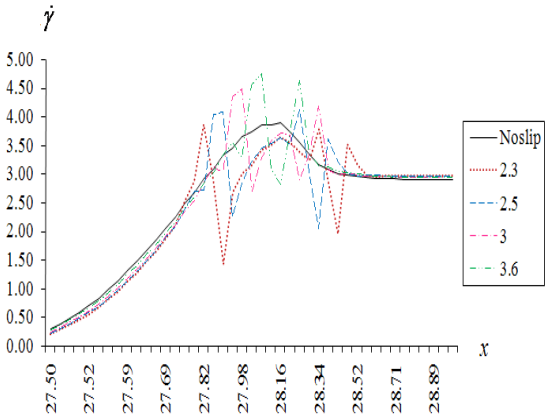

Fig.4. $\dot{\gamma}$ with variation of II at α=1.0, Newtonian fluid.

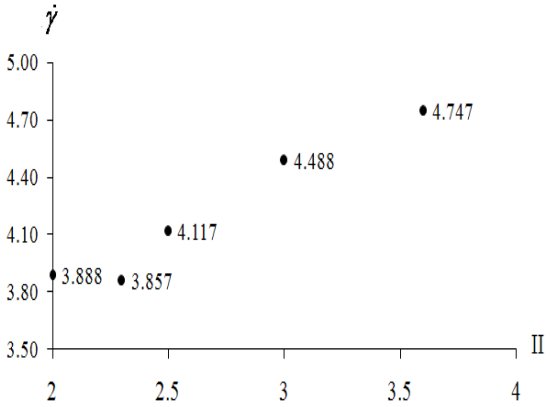

Fig.5. The peak of $\dot{\gamma}$ with variation of II at α=1.0, Newtonian fluid.

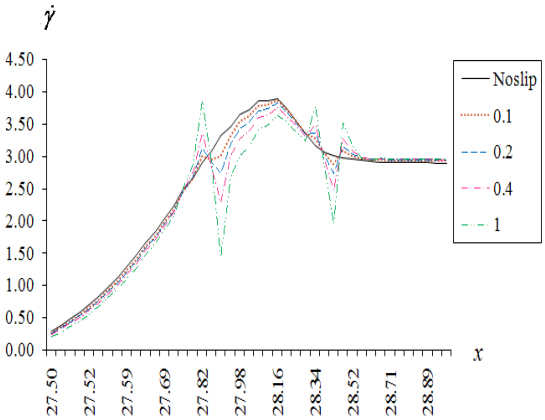

Fig.6. The peak of $\dot{\gamma}$ with variation of α at II=2.3, Newtonian fluid.

The streamline contours of Newtonian fluids for the no-slip and the slip cases at α=0.1 and II=2.3 are shown in Figures 7(a) and 7(b), respectively. The simple observation of the vortex around the corner contraction for the no-slip velocity looks more acute than the figure shown for the slip case.

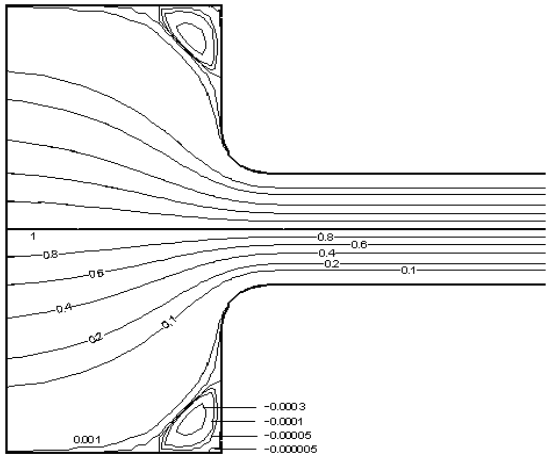

(a) No slip

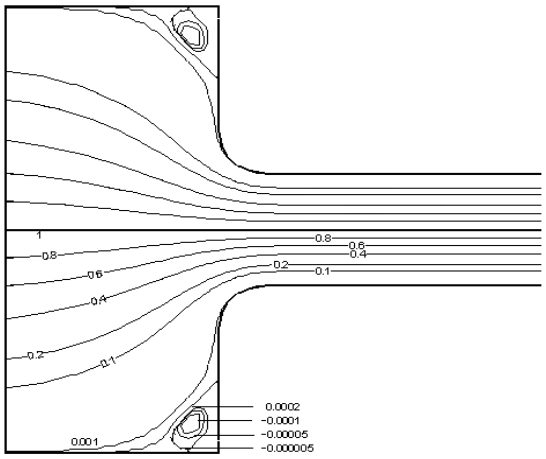

(b) Slip

Fig.7. Streamline contour of Newtonian fluid.

As stated above for the reason why II = 2.3 is used to display final solution, Figure 8 depicts the line contours under the slip condition for α = 0.1. This behavior can be explained as follows. Figure 8(a) displays the horizontal velocity u_x of the parabolic line shape, which shows the maximum value at the symmetry line and the vortex appears at

the corner while Figure 8(b) shows the line contour of the vertical velocity v_y with the maximum value being near the location of the sharp corner contraction where the fluid pass through the sudden change in geometry from 4 unit reduce to 1 unit. Figure 8(c) represents the line contour of pressure p that shows the maximum value at the inlet boundary then gradually declines along a path of the abrupt change in geometry.

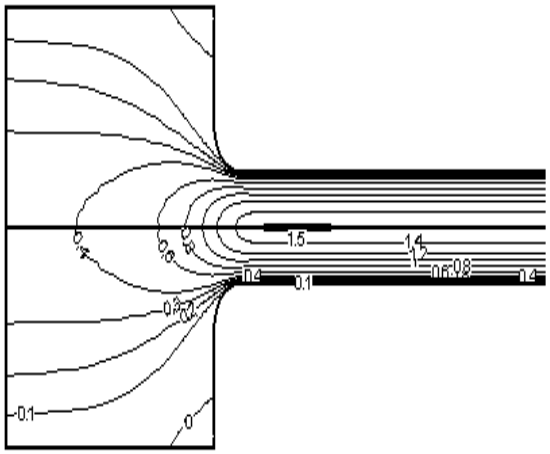

(a) u_x

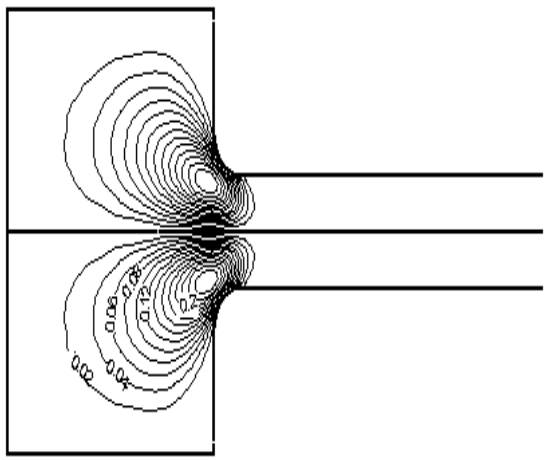

(b) v_y

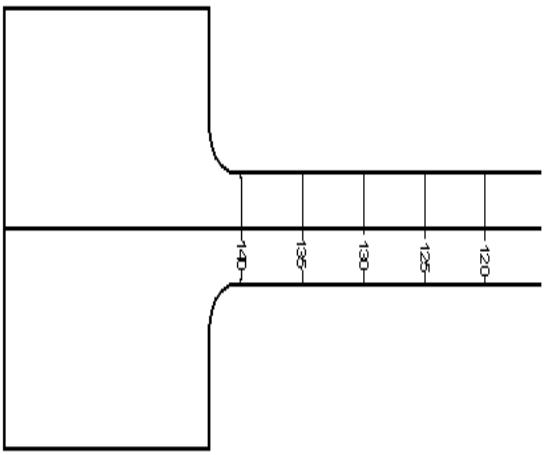

(c) p

Fig.8. Line contour with slip at α=0.1, II=3.3.

6. Conclusion

For steady-state viscoelastic flows in 4:1 contraction rounded geometry through planar isothermal Newtonian fluids, the semi-implicit Taylor-Galerkin pressure-correction finite element scheme is employed to solve the nonlinear partial differential equation for stick before the Phan-Thien slip rule is added to calculate the velocity at the channel wall. After critical II was adjusted, the slip coefficient of Newtonian fluids with rounded corner meshes is determined to have an optimum value of 0.1. In the case of the right selection for the second invariant, this proper slip coefficient reduces the peak of the shear rate and the vortex size since the velocity at the wall forces the fluids to follow a smooth path and yield a more stable outcome. In addition, the higher values for α and II cause stronger oscillations akin to the phenomenon of shark skins.

7. Acknowledgments

The authors would like to thank the scholarship from National Science and Technology Development Agency (NSTDA), Thailand to support PhD degree. We also

thank the Advanced Virtual and Intelligence Computing (AVIC) at the Department of Mathematics and Computer Science, Faculty of Science, Chulalongkorn University for the computing resources.

8. References

[1] Walters, K. and Rawlinson, D.M., On some Contraction Flows for Boger fluids, Rheol. Acta, Vol.21, pp.547-552, 1982.

[2] Boger, D.V., Viscoelastic Flows through Contractions, Ann. Rev. Fluid Mech, Vol.19 , pp.157–182, 1987.

[3] Phillips, T.N. and Williams, A.J., Viscoelastic Flow through a Planar Contraction using a Semi-Lagrangian Finite Volume Method, J. Non-Newtonian Fluid Mech, Vol.87, pp.215–246, 1999.

[4] Phillips, T.N. and Williams, A.J., Comparison of Creeping and Inertial Flow of an Oldroyd B Fluid through Planar and Axisymmetric Contractions, J. Non-Newtonian Fluid Mech, Vol.108, pp.25–47, 2002.

[5] Aboubacar, M. and Webster, M.F., A Cell-Vertex Finite Volume/Element Method on Triangles for Abrupt Contraction Viscoelastic Flows, J. Non-Newtonian Fluid Mech, Vol.98, pp.83–106, 2001.

[6] Aboubacar, M., Matallah, H. and Webster, M.F., Highly Elastic Solutions for Oldroyd-B and Phan-Thien/Tanner Fluids with a Finite Volume/Element Method : Planar Contraction Flows, J. Non-Newtonian Fluid Mech, Vol.103, pp.65–103, 2002.

[7] Alves, M.A., Torres, D., Goncalves, M.P., Oliverira, P.J. and Pinho, F.T., On the Effect of Contraction Ratio in Viscoelastic Flow through Abrupt Contractions, J. Non-Newtonian Fluid Mech, Vol.122, pp.117–130, 2004.

[8] Ngamaramvaranggul, V. and Webster, M.F., Viscoelastic Simulation of Stick-Slip and Die-Swell Flows, Int. J. Num. Meth. Fluids, Vol.36, pp.539-595, 2001.

[9] Ngamaramvaranggul, V. and Webster, M.F., Simulation of Pressure-Tooling Wire-Coating Flow with Phan-Thien/Tanner Models, Int. J. Num. Meth. Fluids, Vol.38, pp.677-710, 2002.

[10] Silliman, W.J. and Scriven, L.E., Separating Flow near a Static Contact Line : Slip at a Wall and Shape of a Free Surface, J. Comp. Phys, Vol.34, pp.287-313, 1980.

[11] Ramamurthy, A.V., Wall Slip in Viscous Fluids and Influence of Materials of Construction, J. Rheol, Vol.30, pp.337-357, 1986.

[12] Phan-Thien, N., Influence of Wall Slip on Extrudate Swell : a Boundary Element Investigation, J. Non-Newtonian Fluid Mech, Vol.26, pp.327-340, 1988.

[13] Ngamaramvaranggul, V. and Webster, M.F., Simulation of Coating Flows with Slip Effects, Int. J. Num. Meth. Fluids, Vol.33, pp.961-992, 2000.

[14] Thongjub, N., Puangkird, B. and Ngamaramvaranggul, V., Simulation of Slip Effects with 4:1 Contraction Flow for Oldroyd-B Fluid, AIJSTPME., Vol.6, No.3, pp. 19-28, 2013.

[15] Ngamaramvaranggul, V. and Thongjub, N., Newtonian Fluid through the Abrupt 4:1 Contraction Flow of Rounded Corner Geometry with Feedback Pressure-Driven Velocity Flow, Int. J. Inf. Tech. Comp. Sc., Vol.15, No.2, pp.1-10, 2014.